19. W. J. Lee, J. D. Lee, V. V. Kravchenko, R. J. Ulevitch, P. T. Brey, *Proc. Natl. Acad. Sci. U.S.A.* **93**, 7888 (1996).
20. C. Ma, M. R. Kanost, *J. Biol. Chem.* **275**, 7505 (2000).
21. M. Ochiai, M. Ashida, *J. Biol. Chem.* **275**, 4995 (2000).
22. M. S. Kim, M. Byun, B. H. Oh, *Nature Immunol.* **4**, 787 (2003).
23. R. Zhang *et al.*, *J. Biol. Chem.* **278**, 42072 (2003).
24. C. A. Janeway, *Cold Spring Harbor Symp. Quant. Biol.* **54**, 1 (1989).
25. S. Rutschmann *et al.*, *Nature Immunol.* **1**, 342 (2000).
26. M. Gottar *et al.*, *Nature* **416**, 640 (2002).
27. A. Bateman *et al.*, *Nucleic Acids Res.* **30**, 276 (2002).
28. We thank our colleagues in the laboratory for critical comments on the manuscript, W.-J. Lee for the kind gift of GNBP1 reagents, J.-M. Ubeda for suggesting the double-overexpression experiment, and M.-C. Lacombe for expert technical help. Supported by CNRS and the Ministère de l'Education Nationale de la Recherche et de la Technologie and by NIH. Requests for the *GNBP1*^{osi} (e03371) stock should be addressed to Exelixis.

Supporting Online Material
www.sciencemag.org/cgi/content/full/302/5653/2126/DC1
Materials and Methods
SOM Text
Figs. S1 to S3
References and Notes

8 April 2003; accepted 30 October 2003

Kinesin Moves by an Asymmetric Hand-Over-Hand Mechanism

Charles L. Asbury,[1] Adrian N. Fehr,[2] Steven M. Block[1,2]*

Kinesin is a double-headed motor protein that moves along microtubules in 8-nanometer steps. Two broad classes of model have been invoked to explain kinesin movement: hand-over-hand and inchworm. In hand-over-hand models, the heads exchange leading and trailing roles with every step, whereas no such exchange is postulated for inchworm models, where one head always leads. By measuring the stepwise motion of individual enzymes, we find that some kinesin molecules exhibit a marked alternation in the dwell times between sequential steps, causing these motors to "limp" along the microtubule. Limping implies that kinesin molecules strictly alternate between two different conformations as they step, indicative of an asymmetric, hand-over-hand mechanism.

Results from a variety of single-molecule experiments have furnished insights into the mechanochemical properties of kinesin motor proteins. Individual kinesin dimers move processively, making discrete 8-nm steps at stochastic intervals, and may take a hundred or more steps before releasing from the microtubule surface. Processive motion persists even in the presence of sustained external loads up to several pN (*1*–*3*), suggesting that some portion of the kinesin dimer remains bound to the microtubule at all times. Kinesin molecules move on the microtubule surface lattice along paths parallel to the protofilaments (*4*, *5*), interacting with one binding site per tubulin dimer (*6*). Finally, kinesin moves in such a way as to hydrolyze exactly one adenosine triphosphate (ATP) molecule per 8-nm step (*1*, *7*, *8*). Two broad classes of stepping pattern are consistent with the foregoing observations: hand-over-hand models, in which the two heads step alternately, exchanging leading and trailing roles with each step, and inchworm models, in which a given head remains in the lead (*9*, *10*).

The active portion of the kinesin motor is formed from a dimer of identical heavy chains, which fold into twin heads attached to a single common stalk (*11*). The two globular heads, which carry enzymatic activity and bind ATP and microtubules, are joined to the stalk through short (~13 amino acids) neck linker regions, consisting of single polypeptide chains (*12*). The heavy chains then intertwine to form a coiled-coil dimerization domain consisting of classic heptad repeats (*11*). On the basis of this structure, free rotation (i.e., swiveling) of an individual head could occur, in principle, about the neck linker, but head motions would be summed mechanically at the point where the heavy chains merge into a common stalk, precluding further independent rotation beyond that point.

A recent study by Gelles and co-workers (*10*) supplied compelling evidence that significant rotation of the kinesin stalk does not occur during stepping. A large rotation, up to 180°, should be imparted to the stalk in a class of hand-over-hand models termed "symmetric." This class is symmetric in the sense that "the three-dimensional structure of the kinesin-microtubule complex is identical at the beginning and end of each ATP hydrolytic cycle, except that. . .the two subunits (and therefore the two heads) swap places" (*10*). An example of a symmetric hand-over-hand model with this property is one in which the dimer rotates about an axis perpendicular to the microtubule by half a revolution per step (*13*). On the basis of their negative findings, Hua *et al.* (*10*) ruled out the so-called symmetric hand-over-hand model, and instead proposed an inchworm mechanism wherein only one of the kinesin heads is active in hydrolyzing ATP, to account for the observation of one ATP hydrolysis per 8-nm step (*1*, *7*, *8*). However, the possibility of an asymmetric hand-over-hand motion was not formally excluded, provided that compensatory movements of the head and neck linker domains during stepping conspire to suppress the overall rotation of the common stalk. One such asymmetric mechanism has been proposed, for example, in which the kinesin-microtubule complex alternates between two conformations and the stepping motions of the two heads are distinctly different (*14*).

To discriminate among candidate models, we measured the stepwise motion of individual native and recombinant kinesin homodimers at high spatiotemporal resolution, using an optical force-clamp apparatus (*2*, *3*, *15*, *16*). We found that the intrinsic stepping rates can alternate between two different values at each sequential step, causing kinesin molecules to "limp." The strict kinetic alternation in stepping implies an alternation between two underlying molecular configurations, thereby excluding fully symmetric models, such as the inchworm and symmetric hand-over-hand mechanisms. Therefore, the discovery that kinesin limps, taken together with its other nanomechanical properties, implies that it advances by some form of asymmetric hand-over-hand mechanism. Recent work has established that an actin-based motor, myosin V, also moves hand-over-hand (although it is not yet known whether the motion is symmetric or asymmetric), raising the possibility that the mechanism may be common to dimeric, processive mechanoenzymes (*17*).

In our assays (*18*), we attached single kinesin molecules to microscopic beads (0.5 μm diameter) that served as markers for position and as handles to apply external forces (*1*–*3*, *15*, *16*, *19*, *20*). Using an optical trap, we captured individual freely diffusing beads carrying kinesin motors and placed them near microtubules immobilized on a cover glass, whereupon they bound and moved. Subsequent processive motion was tracked with nanometer-level precision. We used a feedback-controlled force clamp to apply a constant rearward load during motion, at a level below the kinesin stall force (~6 pN) (*20*–*22*), an arrangement that greatly reduces Brownian fluctuations and improves spatiotemporal resolution (*2*, *3*). The force clamp also allows comparatively long displacements to be scored (up to ~40 steps), facilitating statistical analysis. We studied

[1]Department of Biological Sciences, [2]Department of Applied Physics, Stanford University, Stanford, CA 94305, USA.

*To whom correspondence should be addressed. E-mail: sblock@stanford.edu

the motions of His- and biotin-tagged recombinant kinesin derivatives of various lengths from fruit fly and human expressed in *Escherichia coli*, as well as native kinesin purified from squid.

A truncated derivative of *Drosophila melanogaster* kinesin (DmK401) containing two identical heads and a sufficient length of neck coiled-coil for dimerization (*23*) exhibited an obvious limp, alternating between slow and fast dwell times (where dwell times are defined as the time intervals between successive 8-nm advances). Characteristically, limping manifested itself as a tendency for steps in position recordings to occur in discrete pairs (Fig. 1A), even though individual dwell times are governed by a stochastic process and therefore show variability. Put somewhat differently, when the dwell times in any given record were numbered sequentially, the longer-lived dwell times tended to cluster systematically in either the even- or the odd-numbered subset. This clustering was not an experimental artifact, because limping was almost never observed with native kinesin protein purified from *Loligo pealei* (LpK) and studied under the same conditions (Fig. 1B).

Statistical analysis showed that the average dwell times for the slow and fast phases of DmK401 stepping were significantly different. Because the starting phase in any given record is not known a priori, the dwell intervals were assigned to either a "slow" or a "fast" phase by comparing the mean duration of the even-numbered subset of intervals to the mean duration of the odd-numbered subset for each record. All intervals in the subset with the greater mean were assigned to the slow phase; conversely, those from the subset with the lesser mean were assigned to the fast phase. Having made such an assignment for every record, we could then combine data from an ensemble of single molecules to generate global distributions for the fast and slow phases (Fig. 2A). The durations of both the slow and fast dwell times for DmK401 were distributed nearly exponentially (*24*) but with characteristic lifetimes that differed nearly sixfold, $\tau_{slow} = 136 \pm 6$ ms and $\tau_{fast} = 24 \pm 1$ ms. This disparity was also reflected in the limp factor, L, defined as the ratio of the mean duration of the slow phase to that of the fast phase in a given record (*25*). The distribution of L showed significant limping in most individual molecules but varied widely from bead to bead (and even from run to run): 63% of records had $L > 4$, and the average limp factor was $\overline{L} = 6.45 \pm 0.31$ (Fig. 2B). Some individual DmK401 motors taking multiple runs generated consistently higher limp factors than did others, but the global distribution was broad and did not contain clearly separable populations of limping versus nonlimping molecules.

In contrast to the clear-cut limping displayed by DmK401, limping was nearly absent from stepping records of native squid kinesin (Fig. 1B). The identical method of phase assignment was applied to generate global distributions for the slow and fast phase of stepping in LpK (Fig. 2C). The dwell times were again distributed nearly exponentially but with characteristic lifetimes, $\tau_{slow} = 90 \pm 4$ ms and $\tau_{fast} = 54 \pm 2$ ms, which differ far less than those of DmK401. Furthermore, the limp factors for LpK were distributed quite narrowly (compare Fig. 2, B and D), with just 8% of runs producing $L > 4$. The average limp factor was $\overline{L} = 2.23 \pm 0.14$, which is only slightly higher than the value anticipated for a nonlimping stepper, estimated by computer simulations to be $\overline{L} \sim 1.8$.

We note that the systematic assignment of even or odd dwell intervals to either a slow or a fast phase introduces sampling bias for records of finite length, even when all the stepping times are drawn from the same statistical distribution. This bias occurs because the subset with the maximum sum is always selected for one phase and the minimum for the other. The sampling bias becomes negligible only in the limit of long runs containing a great many individual steps, or when the difference between the two phases is large compared with the stochastic variation in dwell times (as with DmK401). For shorter runs containing fewer steps on average, however, the bias can be estimated. Computer-simulated records for an ideal random stepper were analyzed, i.e., for a nonlimping Poisson process with dwell intervals drawn from a single exponential distribution (with lifetime $\tau = 71$ ms) (*26*). For such a simulation, we obtained $\overline{L}, = 1.79 \pm 0.14$, with $\tau_{slow} = 87 \pm 3$ ms and $\tau_{fast} = 56 \pm 2$ ms (Fig. 2, E and F), values quite similar to LpK.

We then tested a series of recombinant kinesin derivatives from *Drosophila* of increasing stalk length (Fig. 3A). As longer and longer sections of the coiled-coil stalk region were included in the expressed construct, the propensity to limp decreased monotonically (Fig. 3B). The largest construct tested, DmK871 (which includes 90% of the heavy chain), had a limp factor of 2.16 ± 0.17, statistically indistinguishable from native squid kinesin. Interestingly, the systematic

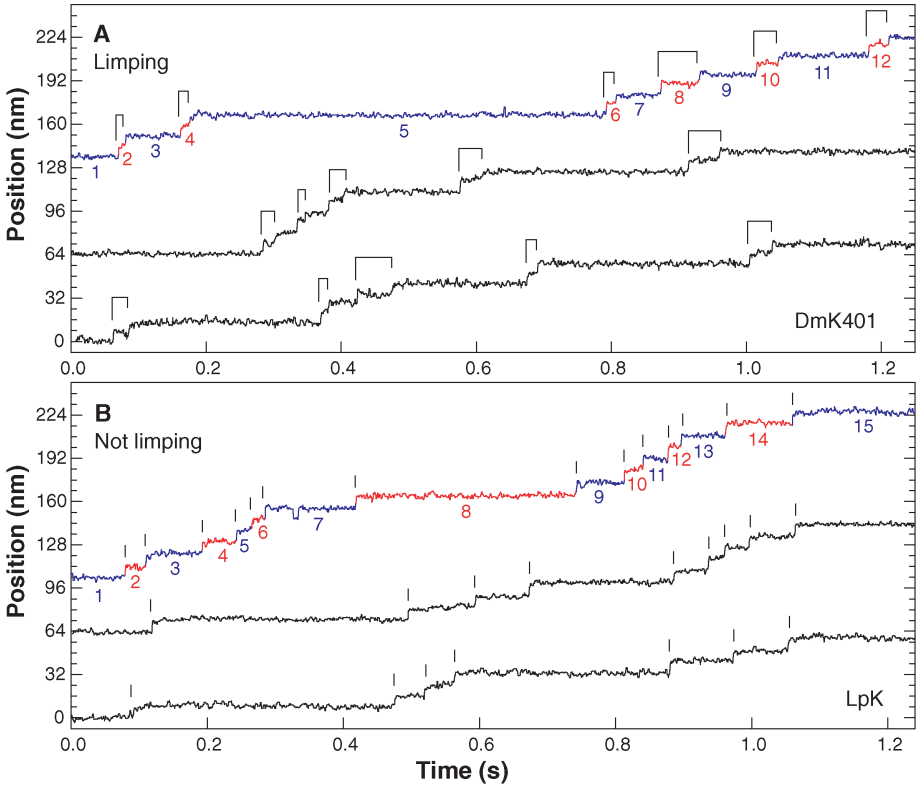

Fig. 1. Representative high-resolution stepping records of position against time, showing the single-molecule behavior of kinesin motors under constant 4 pN rearward loads. (**A**) Limping motion of the recombinant kinesin construct, DmK401. The dwell intervals between successive 8-nm steps alternate between slow and fast phases, causing steps to appear in pairs, as indicated by the ligatures. (**B**) Nonlimping motion of native squid kinesin, LpK. No alternation of steps is apparent; vertical lines mark the stepping transitions. Slow and fast phase assignments, as described in the text, are indicated in color on the uppermost trace of each panel (blue and red, respectively), and the corresponding dwell intervals are numbered. All traces were median filtered with a 2.5-ms window.

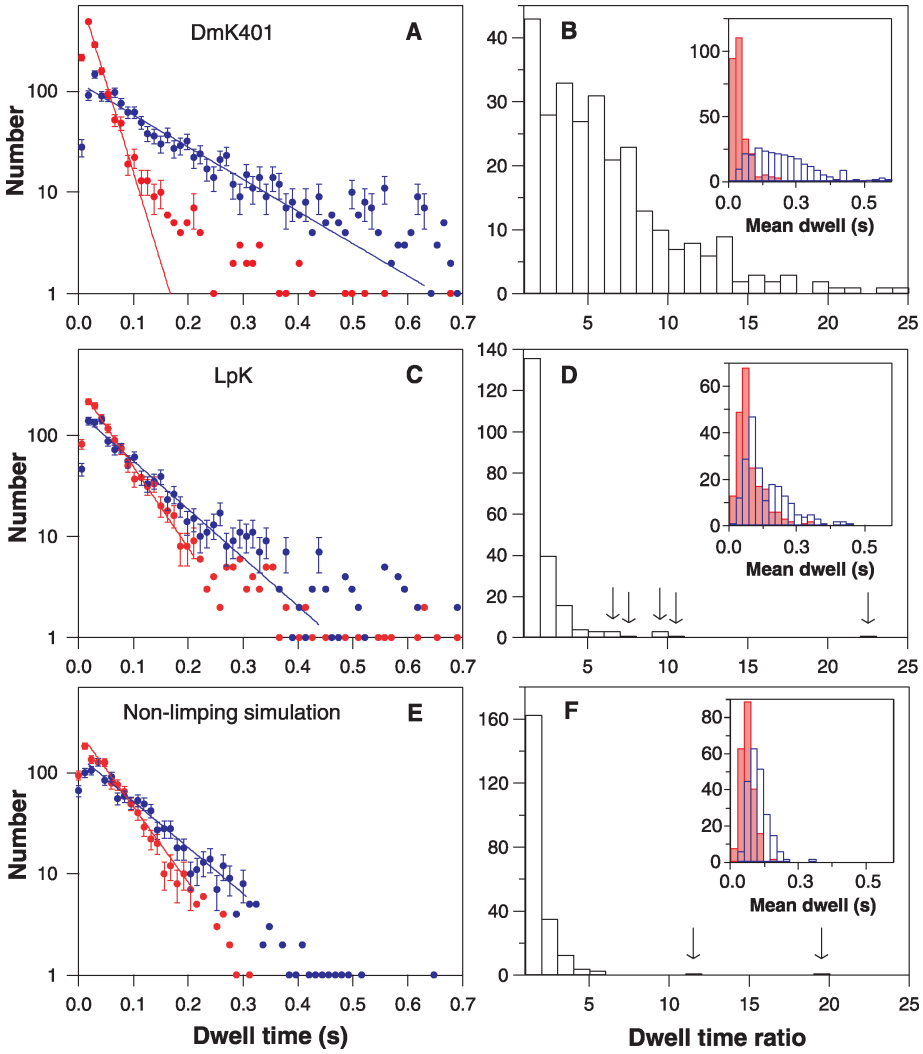

Fig. 2. Stepping statistics for DmK401, LpK, and a computer simulation. (**A**) Experimental dwell time distributions for the slow (blue) and fast (red) phases of DmK401 motion, with statistical errors as indicated. Solid lines show single-exponential fits to the data, with time constants τ_{slow} = 136 ± 6 ms and τ_{fast} = 24 ± 1 ms. The first bin and bins with < 7 counts were not included in fits (these points are displayed without error bars); 2,948 intervals from 278 individual records are represented. (**B**) Experimental distribution of the limp factor, *L*, for individual records of DmK401 movement (black). (Inset) Histograms of the mean durations of the slow (blue) and fast (red) phases for individual records. (**C**) Same as in (A), but for LpK. The time constants are τ_{slow} = 90 ± 4 ms and τ_{fast} = 54 ± 2 ms. 2,523 dwells from 208 records are represented. (**D**) Same as in (B), but for LpK. Outliers with *L* > 6 (arrows) are caused by rare, limping LpK molecules. (**E**) Same as in (A), but for a computer simulation of an ideal Poisson stepper with a single characteristic stepping time (τ = 71 ms) that produced the time constants τ_{slow} = 87 ± 3 ms and τ_{fast} = 56 ± 2 ms. 2,230 dwells from 220 records are represented. (**F**) Same as in (B), but for the simulation.

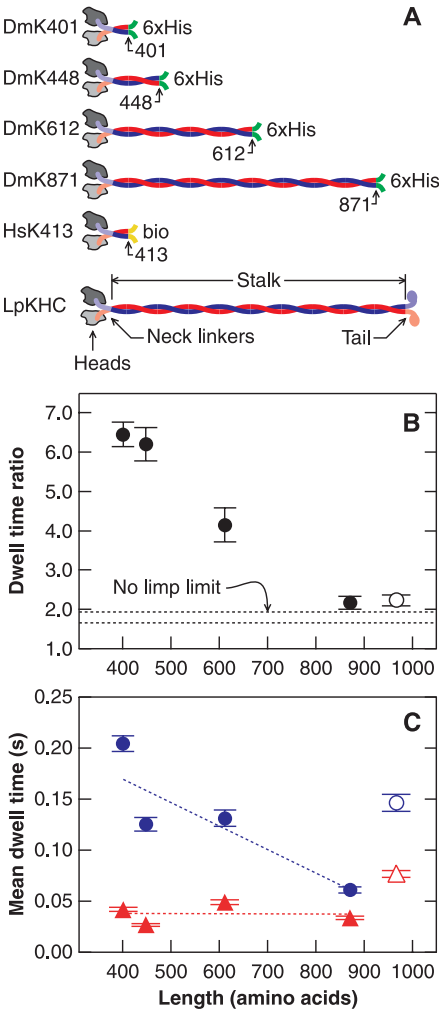

Fig. 3. The effect of construct length on kinesin limping. (**A**) Cartoons showing the named structural features of kinesin dimers used in this work, with stalk lengths displayed approximately to scale and numbers of amino acids shown. (**B**) The mean limp factors, *L*, for DmKHC constructs (black circles), full-length native LpK (open circle), and for a nonlimping Poisson stepper under conditions similar to our experiments (dashed lines, showing 63% confidence intervals), as a function of the construct length (number of amino acids). Points show the means and estimated errors [evaluated by bootstrapping (*35*)] for each distribution of not less than 141 limp factors. (**C**) The average durations of the slow (blue circles) and fast stepping phases (red triangles) as functions of the construct length for DmKHC derivatives (solid symbols) and native LpK (open symbols).

increase in limp factor with shorter stalk length was attributable to an increase in the characteristic lifetime of the slow phase of stepping, whereas the timing of the fast phase appeared to remain invariant (Fig. 3C). This result suggests that the kinetics for one head alone are slowed in limping constructs, whereas the partner head retains normal enzymatic activity.

Limping was not restricted to recombinant *Drosophila* kinesin molecules. A bacterially expressed derivative of human kinesin with a C-terminal biotinylation tag (HsK413) (*27*) also limped. HsK413 produced a limp factor of 2.98 ± 0.25, significantly greater than that for a Poisson stepper or native squid kinesin but not as pronounced as the two comparably sized fruit fly constructs, DmK401 and DmK448 (Fig. 3B). On rare occasions (9 of 208 records), even selected squid kinesin molecules appeared to limp, producing outliers in Fig. 2D (arrows). Some of these outlier molecules limped consistently (*28*).

The fact that both native and bacterially expressed kinesin homodimers from several species can limp suggests that this behavior may reflect the common mechanism by which all processive kinesin molecules move. The alternation between short and long dwell times during limping directly reflects a corresponding alternation in the intrinsic rate for exiting the dwell state. This strict kinetic switching implies that the structural configuration of the kinesin-microtubule complex at the end of even-numbered dwell intervals differs from that of odd-numbered dwell intervals. Thus, the mechanism whereby kinesin advances must be asymmetric, in the sense that its underlying molecular conforma-

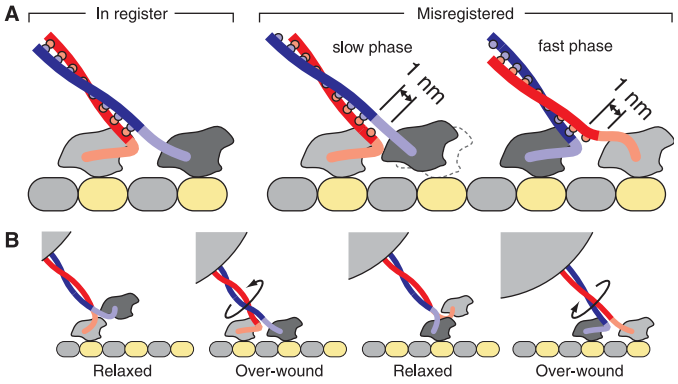

Fig. 4. Candidate models for limping in kinesin. (**A**) The misregistration model. Left (in register): The two-heads-bound state for native, non-limping kinesin, shown as it moves to the right along the microtubule lattice (tubulin $\alpha-\beta$ subunits, spaced pairwise by 8 nm, are indicated in gray and yellow). The coils of both heavy chains (blue and red ribbons) are in correct register. Middle and right (misregistered): A shift in registration of the coiled-coil by a single heptad changes the relative lengths of the head-neck linker regions by up to 1 nm. On alternate steps, this shift places one head (dark gray) farther from its binding site on the microtubule, reducing the stepping rate when this head attempts to take the lead (middle). When the partner head (light gray) steps, the shift is accommodated by slack in the longer tether (right). (**B**) The winding model. When one head (dark gray) steps forward, the neck coiled-coil (red and blue) is overwound relative to the relaxed state. When the partner head (light gray) leads, the coiled-coil is underwound. Asymmetry in torsional compliance slows the stepping associated with overwinding.

tions switch at every step. Symmetric mechanisms—by virtue of their symmetry—cannot account for switching. For example, inchworm-type models will not limp without the ad hoc incorporation of additional (asymmetric) features, nor will symmetric hand-over-hand models of the type discussed by Gelles and co-workers (*10*).

The process by which kinesin motors advance is poorly understood in mechanistic detail, so it is not currently possible to assign limping to established structural features of its motion. However, some candidate mechanisms are immediately suggested by the molecular geometry of the kinesin dimer and its presumed relation to the microtubule during a hand-over-hand walk. Limping might be induced, in principle, in kinesin molecules with an axial misregistration between the α helices of their coiled-coil dimerization domains (*29–31*). Misregistration by a full heptad repeat would shift the globular heads relative to one another, effectively increasing the maximum neck linker length for one head by up to ~1 nm, i.e., from 3 to 4 nm. Such a shift could shorten the tether of the other head, generating an asymmetry. The head with the shorter tether would require additional time to find its forward microtubule binding site in a diffusional search (Fig. 4A), thereby slowing its kinetics relative to the partner head in situations where this step becomes rate-determining. The increased propensity of short constructs to limp, along with their large variation in limp factor, may be explained by their greater likelihood of axial misregistration, arising from the reduced thermodynamic stability of short coiled-coils.

In an alternative picture, limping may be caused by an over- and underwinding of the coiled-coil region generated during hand-over-hand motion (Fig. 4B). Coiled-coils are thought to have an asymmetric torsional compliance because of their chirality (*32*); hence, the energetic barrier (along with the overall energetic cost) for winding the kinesin stalk from its relaxed, equilibrium configuration should differ with the handedness of rotation. In the event that such torsional barriers affect the rates of head advance, they could give rise to kinetic alternation. The relative difference in barrier height should be reduced with longer tethers, which are torsionally more compliant, perhaps accounting for the decrease in limping with increasing construct length (*33*).

None of the candidate mechanisms would seem to offer an immediate explanation for the experimental observation that only the time constant for the slow phase of limping is increased in shorter constructs, although such an effect may be incorporated with additional assumptions (*34*). Nevertheless, the mechanisms do suggest experimental approaches that should drive further single-molecule work to explore these possibilities. Regardless of the mechanism giving rise to it, however, the finding that kinesin molecules limp indicates that an asymmetric, hand-over-hand model supplies the correct description of kinesin stepping. Limping behavior may also complicate the interpretation of earlier biochemical kinetic experiments performed on populations of soluble kinesin dimers: Such molecules are generally derived from short, bacterially expressed constructs, in which the kinetic differences between the two heads are most pronounced.

References and Notes

1. M. J. Schnitzer, S. M. Block, *Nature* **388**, 386 (1997).
2. K. Visscher, M. J. Schnitzer, S. M. Block, *Nature* **400**, 184 (1999).
3. S. M. Block, C. L. Asbury, J. W. Shaevitz, M. J. Lang, *Proc. Natl. Acad. Sci. U.S.A.* **100**, 2351 (2003).
4. J. Gelles, B. J. Schnapp, M. P. Sheetz, *Nature* **331**, 450 (1988).
5. S. Ray, E. Meyhofer, R. A. Milligan, J. Howard, *J. Cell Biol.* **121**, 1083 (1993).
6. Y. H. Song, E. Mandelkow, *Proc. Natl. Acad. Sci. U.S.A.* **90**, 1671 (1993).
7. W. Hua, E. C. Young, M. L. Fleming, J. Gelles, *Nature* **388**, 390 (1997).
8. D. L. Coy, M. Wagenbach, J. Howard, *J. Biol. Chem.* **274**, 3667 (1999).
9. K. Svoboda, P. P. Mitra, S. M. Block, *Biophys. J.* **68**, 69S (1995).
10. W. Hua, J. Chung, J. Gelles, *Science* **295**, 844 (2002).
11. R. D. Vale, R. J. Fletterick, *Annu. Rev. Cell Dev. Biol.* **13**, 745 (1997).
12. S. Rice *et al.*, *Nature* **402**, 778 (1999).
13. J. Howard, *Annu. Rev. Physiol.* **58**, 703 (1996).
14. A. Hoenger *et al.*, *J. Mol. Biol.* **297**, 1087 (2000).
15. M. J. Lang, C. L. Asbury, J. W. Shaevitz, S. M. Block, *Biophys. J.* **83**, 491 (2002).
16. K. Visscher, S. M. Block, *Methods Enzymol.* **298**, 460 (1998).
17. A. Yildiz *et al.*, *Science* **300**, 2061 (2003).
18. Materials and methods are available as supporting material on *Science* Online.
19. K. Svoboda, C. F. Schmidt, B. J. Schnapp, S. M. Block, *Nature* **365**, 721 (1993).
20. K. Svoboda, S. M. Block, *Cell* **77**, 773 (1994).
21. E. Meyhofer, J. Howard, *Proc. Natl. Acad. Sci. U.S.A.* **92**, 574 (1995).
22. H. Kojima, E. Muto, H. Higuchi, T. Yanagida, *Biophys. J.* **73**, 2012 (1997).
23. E. Berliner, E. C. Young, K. Anderson, H. K. Mahtani, J. Gelles, *Nature* **373**, 718 (1995).
24. In the limit of very high loads approaching stall, or very low ATP concentrations, dwell intervals for kinesin are distributed exponentially because the stepping rate is dominated by a single rate-determining transition in the biochemical cycle (*1–3*). Under the conditions of the current work (4 pN rearward load and 2 mM ATP), the dwell interval distributions are expected to deviate slightly from pure exponentials (*2*, *3*).
25. The limp factor, *L*, is a statistic derived from each individual record. The ratio of fast to slow phase lifetimes is an ensemble statistic derived from the combined data for many such records. The average limp factor therefore provides an alternative measure of the overall stepping asymmetry. Its expectation value is not identical to the global lifetime ratio because of the effect of finite run lengths.
26. The simulations contained runs with numbers of steps chosen to match closely those in our experiments (*18*).
27. S. S. Rosenfeld, P. M. Fordyce, G. M. Jefferson, P. H. King, S. M. Block, *J. Biol. Chem.* **278**, 18550 (2003).
28. For example, one such molecule generated 21 runs in all, 13 of which included more than eight dwell intervals, and were therefore scored (*18*). This molecule accounted for three of the nine outliers with $L > 6$, and the average limp factor for the molecule was 4.7.
29. K. M. Misura, R. H. Scheller, W. I. Weis, *J. Biol. Chem.* **276**, 13273 (2001).
30. B. Tripet, R. D. Vale, R. S. Hodges, *J. Biol. Chem.* **272**, 8946 (1997).
31. Y. Li *et al.*, *Nature* **424**, 341 (2003).
32. Z. Bryant *et al.*, *Nature* **424**, 338 (2003).
33. One quantity that varies systematically with the length of the construct in our experiments is the angle, θ, between the microtubule axis and the kinesin stalk, which experiences a force on its distal end acting through the center of the attached bead (fig. S2). This force has both rearward and upward components, and Howard and colleagues (*13*) have shown that the speed of kinesin movement can be affected by changes in the upward force. For the constructs used here, we estimate that θ ranges from 45° to 63° (table S1), which corresponds to a 26% maximal variation in upward loading, seemingly too small to account for a threefold change in limp factor. Moreover, small changes in loading would not be expected a priori to affect the two heads differentially.
34. For example, an asymmetric effect on the characteristic step times for limping constructs could be explained in the misregistration model by assuming that for correctly dimerized molecules, the

rates of stepping are not normally limited by the rates at which heads can locate new binding sites. In the case of misregistration, however, the head with the shorter tether takes additional time to reach its new site, thereby slowing its rate of advance to such an extent that it becomes rate-determining for the slow phase. Correspondingly, the head with the longer tether takes less time to advance, but because this is not the limiting factor, there is no significant variation in the fast phase. A similar explanation could be invoked to explain asymmetry in the winding model. A high energetic penalty for overwinding could cause the slow step to become rate-determining, whereas the low penalty for underwinding could have little effect on the fast phase, during which other unidentified transitions would govern the stepping rate.

35. B. F. J. Manly, *Randomization, Bootstrap, and Monte Carlo Methods in Biology* (Chapman & Hall/CRC, Boca Raton, FL, 2001), pp. 34–67.
36. This study was initiated by C.L.A. but subsequently carried out with equal contributions from A.N.F and C.L.A. in the laboratory of S.M.B. We thank J. Gelles, W. Hancock, and S. Rosenfeld for generously providing expression plasmids and kinesin protein, and C. Spiess for assistance with protein expression. B. Weis, P. Harbury, D. Donoho, M. Filler, K. Slon, and members of our laboratory provided helpful advice and discussions. C.L.A. is supported by the Cancer Research Fund of the Damon Runyon-Walter Winchell Foundation (Fellowship DRG-1649). A.N.F. is supported by a Predoctoral Fellowship from the NSF. This work was supported by a grant from the National Institute of General Medical Sciences to S.M.B.

Supporting Online Material
www.sciencemag.org/cgi/content/full/1092985/DC1
Materials and Methods
Figs. S1 and S2
Table S1
References and Notes

27 September 2003; accepted 24 November 2003
Published online 4 December 2003;
10.1126/science.1092985
Include this information when citing this paper.

A *C. elegans* CLIC-like Protein Required for Intracellular Tube Formation and Maintenance

Katherine L. Berry,[1] Hannes E. Bülow,[1] David H. Hall,[2] Oliver Hobert[1]*

The *Caenorhabditis elegans* excretory canal is composed of a single elongated and branched cell that is tunneled by an inner lumen of apical character. Loss of the *exc-4* gene causes a cystic enlargement of this intracellular tube. *exc-4* encodes a member of the chloride intracellular channel (CLIC) family of proteins. EXC-4 protein localizes to various tubular membranes in distinct cell types, including the lumenal membrane of the excretory tubes. A conserved 55–amino acid domain enables EXC-4 translocation from the cytosol to the lumenal membrane. The tubular architecture of this membrane requires EXC-4 for both its formation and maintenance.

The morphogenesis of biological tubes is central to the development of a wide variety of metazoan structures, from the simplest Cnidarian body plans to the vertebrate respiratory, excretory, and circulatory systems. Although biological tubes form by such distinct processes as the hollowing of single cells and the folding of epithelial sheets, in each case an inner lumen is surrounded by a surface of apical character generated by the polarized movement or growth of vesicles or vacuoles (*1*, *2*). However, the molecular mechanisms of tube formation and subsequent maintenance are not well understood.

A simple model of unicellular tube morphogenesis is provided by the *Caenorhabditis elegans* excretory cell, a single cell that forms the major tubular component of the four-cell nematode excretory system (*3*, *4*). This cell extends branched processes, termed canals, along the length of the body on the basolateral surface of the epidermis (Fig. 1A). These processes are tunneled by an inner lumen that is closed at its four endings and is presumed to collect fluids and waste, which it then empties into the excretory duct (*5*). In *exc* (for excretory canal abnormal) mutants, the tubular structure of the excretory cell lumen is disrupted by swellings termed cysts that have been proposed to model tubulocystic kidney disease (*6*). The disruption of tubular morphology in *exc-4* mutants has been previously described as a cystic enlargement of the canal's interior lumen (*6*). Using green fluorescent protein (GFP) markers that specifically label either the cytoplasm or the apical surface of the canal, we confirmed that in the *exc-4* null allele *rh133*, the morphology of the apical surface is altered from a single, long, narrow tube to a set of large, closely packed cystic enlargements, some of which may be disconnected spheres (Fig. 1B) (*7*).

We used single-nucleotide polymorphisms to map the *exc-4* locus to a 130-kb interval on chromosome I and found that a polymerase chain reaction product encompassing the coding region of a predicted intracellular ion channel protein fully rescued the mutant phenotype (*7*). Molecular lesions in this putative channel protein are present in all three *exc-4* mutant alleles—*rh133*, *n561*, and *n2400* (Fig. 1C)—which appear similar in the severity of the excretory phenotype (94 to 100% of animals were defective; $n > 30$). The *rh133* allele has an amber mutation in its sixth residue and therefore presumably eliminates all protein function.

The protein encoded by the *exc-4* locus is one of two *C. elegans* orthologs of the human CLIC family of proteins (Fig. 1D). Members of this family are small proteins that have the unconventional property of translocating from a globular cytosolic form (*8*) to an integral membrane form with chloride channel activity (*9*, *10*). Although it cannot formally be excluded that CLIC proteins are channel-associated rather than pore-forming proteins, the observations that they confer chloride conductance to transfected cells (*8*, *11–16*) and that they are alone sufficient to self-insert into microsomes to form chloride-conducting ion channels (*17–19*) indicate that CLIC proteins are important integral components of a chloride channel. In cell and tissue culture systems, different CLIC family members localize to distinct sets of intracellular membranes, including the endoplasmic reticulum, Golgi apparatus, nuclear membrane, large dense core vesicles, secretory vesicles, and sometimes the plasma membrane, and they are expressed in many different tissue types (*9*, *20*). An understanding of the physiological role of CLICs has been lacking because of the previous absence of animal models. Such a model is now provided by *exc-4* mutant animals.

We examined the expression pattern and subcellular localization of *exc-4* with fluorescent reporter gene technology (*7*). The *gfp*-tagged genomic *exc-4* locus, which is capable of rescuing the *exc-4* mutant phenotype (*7*), shows expression in the excretory system, hypodermis, vulva, pharyngeal muscle, rectal gland, tubular rectal epithelial cells, and tubular neuronal support cells in the head and tail (Fig. 2) (*21*). EXC-4 protein showed highly specific patterns of subcellular localization. In the excretory system, EXC-4 localizes to the lumenal membrane of the excretory cell, the duct,

[1]Department of Biochemistry and Molecular Biophysics, Center for Neurobiology and Behavior, Columbia University, College of Physicians and Surgeons, New York, NY 10032, USA. [2]Department of Neuroscience, Center for *C. elegans* Anatomy, Albert Einstein College of Medicine, Bronx, NY 10461, USA.

*To whom correspondence should be addressed. E-mail: or38@columbia.edu

***Science* Supporting Online Material**

Charles L. Asbury, Adrian N. Fehr, & Steven M. Block, *Kinesin Moves by an Asymmetric Hand-over-Hand Mechanism*

Materials and Methods

Protein preparation. We created expression plasmids for four homodimeric, His-tagged derivatives of *Drosophila melanogaster* kinesin heavy chain (DmKHC) by cassette mutagenesis of previously existing plasmids. pEY4, pVR2 and pSK4 code for three derivatives that include the N-terminal 401, 448 and 612 amino acids of DmKHC, respectively, fused at their C-termini to an 87-amino acid biotinylation peptide (BCCP), (gifts of J. Gelles, Brandeis University (*1, 2*)). To create His-tagged versions, the BCCP sections were replaced by digestion at flanking restriction sites and the subsequent ligation of a synthetic 36-bp cassette containing an in-register hexa-histidine sequence. A fourth plasmid was created from pPK113, which codes for full-length DmKHC (gift of W. Hancock, Pennsylvania State University (*3, 4*)), by similarly replacing the C-terminal 356 bp with a 28-bp hexa-histidine cassette. The accuracy of the resulting plasmids, pCA1, pAF1, pAF2 and pAF3 (coding for DmK401, DmK448, DmK612 and DmK871, respectively) was verified by DNA sequencing.

BL21(DE3) *E. coli* were transformed to create expression strains. Subsequent harvests were essentially as described (*2, 3*), except that mid-log cultures were brought to room temperature upon 1 mM IPTG induction, grown for 3 h before adding 0.2 mM rifampicin and incubated overnight. Pelleted cells were resuspended in lysis buffer (30 mM imidazole, pH 6.7, 4 mM $MgCl_2$, 2 mM DTT, 2 mM EGTA, 2 mM PMSF, 2 μg ml^{-1} pepstatin A, 20 μg ml^{-1} TPCK, 20 μg ml^{-1} TAME, 2 μg ml^{-1} leupeptin, 20 μg ml^{-1} soybean trypsin inhibitor), lysed in a French

Press, and clarified by ultra-centrifugation (170,000 g, 40 min, 4°C). DmK401 was purified to near-homogeneity by binding to nickel-NTA resin (Qiagen) and eluting with > 100 mM imidazole (*3*). No difference in stepping statistics occurred when clarified lysate was used in motility assays, rather than pure DmK401. Therefore most assays were performed with clarified lysate. HsK413, a human Cysteine-light mutant terminated with a 15-amino acid biotinylation peptide, was also used in motility assays (gift of S. Rosenfeld, University of Alabama (*5*)). Native LpK was purified from optic lobes, as in previous work (*6-9*). Only the heavy chains (LpKHC) are represented in Fig. 3a, although some motors are expected to have associated light chains.

***In vitro* motility assays.** Highly dilute preparations of kinesin were mixed with 0.5-μm diameter beads in assay buffer (80 mM Pipes, pH 6.9, 50 mM potassium acetate, 4 mM $MgCl_2$, 2 mM DTT, 1 mM EGTA, 7 μM Taxol and 2 mM ATP) and incubated for > 1 h to allow motor binding. To bind the His-tagged motors, DmK401, DmK448, DmK612 and DmK871, streptavidin-coated polystyrene microspheres (Bangs Laboratories Inc., and Spherotech Inc.) were further functionalized by incubation with biotinylated penta-His antibody (Qiagen) and washed five times in assay buffer prior to mixing with motors. The same beads without antibody were used to bind biotinylated HsK413. LpK was bound non-specifically to silica beads (*7-10*).

Using the optical trap, each bead was positioned near a taxol-stabilized microtubule fixed to a polylysine-coated coverslip. Kinesin-induced displacements were monitored with nanometer precision by a quadrant photodetector (*7-12*). The computer-controlled trap was steered with active feedback to deliver a constant 4 pN backward load to the moving bead (*11,*

12). To ensure work in the single-molecule regime, only records from assays in which fewer than half the tested beads moved were analyzed.

Data analysis. Steps in the position records were identified using custom software written in Igor Pro 4.0 (WaveMetrics, Lake Oswego, OR) and all transitions were confirmed or adjusted by eye. Only low-drift records containing distinct steps were analyzed. For a given record, all intervals had to be contiguous and were required to begin and end with a step to be scored: the intervals so identified were then numbered sequentially. The mean durations of the even- and odd-numbered dwell times were used to assign the appropriate subset to either the slow or fast phase. If the mean duration of even-numbered intervals was greater than that of odd-numbered intervals, then all even-numbered intervals in that record were assigned to the slow phase, and *vice versa*. To minimize misidentification of the two phases arising from the stochastic properties of kinesin stepping (which can create a sampling error), only comparatively long records with > 8 dwell intervals were analyzed. Fast and slow phase intervals for all records were pooled separately. For individual records, the limp factor, L, was computed, defined as the ratio of the mean slow-phase dwell time to the mean fast-phase dwell time. All uncertainties are reported as standard errors.

For simulation purposes, we generated artificial, non-limping records where all individual dwell times were drawn at random from a single exponential population. The number of steps in each simulated run was also drawn from an exponential distribution, whose width was chosen to match the shape of the distribution of step numbers in actual kinesin runs scored (mean number of steps per simulated run = 5.2). Just as for the actual kinesin data, only runs containing > 8 dwell intervals were analyzed to minimize sampling bias. For each simulated run, dwell

intervals were assigned collectively to slow or fast phases and limp factors were computed as described. Multiple simulations gave $\overline{L} = 1.79 \pm 0.14$ (based on 50 simulations of 400 runs each). The average limp factor is not unity due to sampling bias in finite records, as described in the text. Artificial limping records were also simulated, with dwell times alternately drawn from two different exponential populations. These limping simulations exhibited values of L significantly greater than the non-limping case.

Supporting Figures

Fig. S1. Stepping statistics for DmK448, DmK612 and DmK871. (**A**) Experimental dwell time distributions for the slow (blue) and fast (red) phases of DmK448 motion, with statistical errors as indicated. Solid lines show single-exponential fits to the data, with time constants $\tau_{slow} = 88.7 \pm 4.1$ ms and $\tau_{fast} = 14.0 \pm 0.6$ ms. The first bin and bins with < 7 counts were not included in fits (points are shown without error bars); 2242 intervals from 176 individual records are represented. (**B**) Experimental distribution of the limp factor, *L*, for individual records of DmK448 movement (black). *Inset*, Histograms of the mean durations of the slow (blue) and fast (red) phases for individual records. (**C**) Same as in (**A**), but for DmK612. The time constants are $\tau_{slow} = 77.3 \pm 3.2$ ms and $\tau_{fast} = 33.9 \pm 1.32$ ms. 2469 dwells from 201 records are represented. (**D**) Same as in (**B**), but for DmK612. (**E**) Same as in (**A**), but for DmK871. The time constants are $\tau_{slow} = 42.8 \pm 1.9$ ms and $\tau_{fast} = 22.8 \pm 0.9$ ms. 1914 dwells from 141 records are represented. (**F**) Same as in (**B**), but for DmK871. (**G**) Same as in (**A**), but for HsK413. The time constants are $\tau_{slow} = 122 \pm 12$ ms and $\tau_{fast} = 50.5 \pm 4.0$ ms. 925 dwells from 89 records are represented. (**H**) Same as in (**B**), but for HsK413.

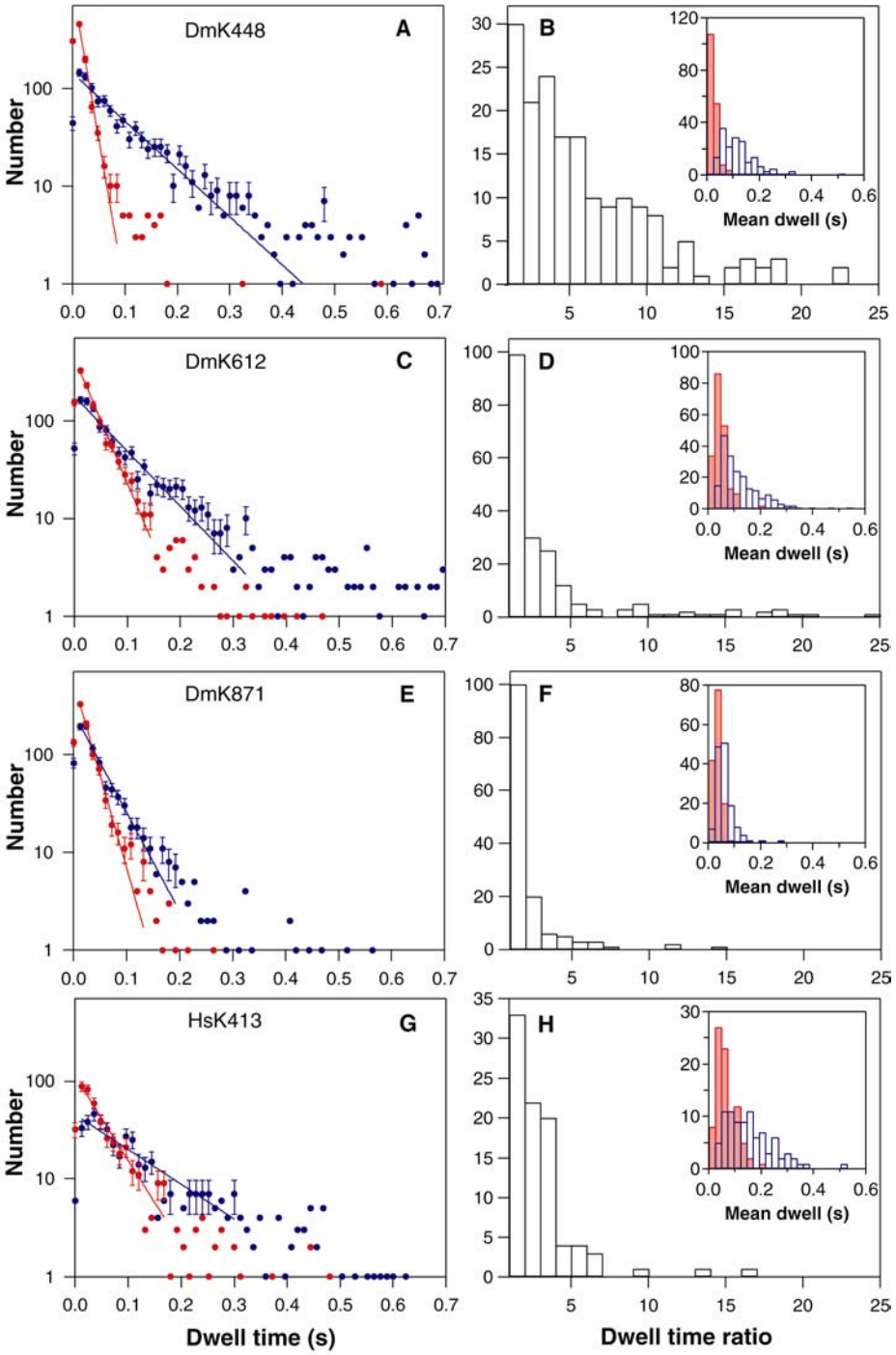
DmK448
A
B
DmK612
C
D
DmK871
E
F
HsK413
G
H
Number
Mean dwell (s)
Dwell time (s)
Dwell time ratio

Figure S1

Fig. S2. Cartoon showing variation in the angle between the stalk and the microtubule axis as the stalk length is changed for DmKHC constructs. The kinesin motors and the bead are displayed approximately to scale.

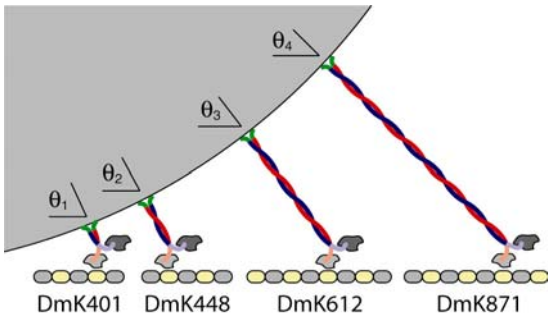

Figure S2

Supporting Table

Table S1. Estimated angle between the microtubule axis and the kinesin stalk for the kinesin constructs used in this work. Construct lengths, *d*, were derived from the number of amino acids in the stalk, assuming 0.15 nm rise per residue (*13*). An extra 20 nm was added for His-tagged constructs (*) to account for additional length provided by the motor-bead linkage, composed of an anti-His antibody plus streptavidin. An extra 10 nm was added for the biotinylated construct (†), linked via streptavidin alone. The angle of applied force, θ, was calculated from $\theta = \sin^{-1}(R/(R+d))$, where R is the bead radius (250 nm).

Construct	*d* (nm)	θ (deg)
DmK401	30*	63
DmK448	37*	60
DmK612	62*	53
DmK871	101*	45
HsK413	23†	66
LpK	88	48

Supporting References

1. J. Gelles *et al.*, *Biophys. J.* **68**, 276S (1995).
2. E. Berliner *et al.*, *J. Biol. Chem.* **269**, 8610 (1994).
3. D. L. Coy, M. Wagenbach, J. Howard, *J. Biol. Chem.* **274**, 3667 (1999).
4. W. O. Hancock, J. Howard, *J. Cell Biol.* **140**, 1395 (1998).
5. S. S. Rosenfeld, P. M. Fordyce, G. M. Jefferson, P. H. King, S. M. Block, *J. Biol. Chem.* **278**, 18550 (2003).
6. R. D. Vale, T. S. Reese, M. P. Sheetz, *Cell* **42**, 39 (1985).
7. K. Visscher, M. J. Schnitzer, S. M. Block, *Nature* **400**, 184 (1999).
8. M. J. Schnitzer, S. M. Block, *Nature* **388**, 386 (1997).
9. S. M. Block, C. L. Asbury, J. W. Shaevitz, M. J. Lang, *Proc. Natl. Acad. Sci. U.S.A.* **100**, 2351 (2003).
10. K. Svoboda, S. M. Block, *Cell* **77**, 773 (1994).
11. K. Visscher, S. M. Block, *Methods Enzymol.* **298**, 460 (1998).
12. M. J. Lang, C. L. Asbury, J. W. Shaevitz, S. M. Block, *Biophys. J.* **83**, 491 (2002).
13. L. Stryer, *Biochemistry, 4th Edition* (W.H. Freeman and Company, New York, 1995), pp. 28-30.